

REF ID: A60000

Copy
RM SL56J22

RESEARCH MEMORANDUM

for the

U. S. Air Force

TRANSONIC AERODYNAMIC CHARACTERISTICS OF A 1/15-SCALE

MODEL OF THE CONVAIR B-58 AIRPLANE

By John M. Swihart

Langley Aeronautical Laboratory
Langley Field, Va.

Declassified by authority of NASA
Classification Change Notices No. [REDACTED]
Dated [REDACTED] 218
JUN 30 1971

[REDACTED]

NATIONAL ADVISORY COMMITTEE
FOR AERONAUTICS

WASHINGTON

OCT 19 1956

[REDACTED]

[REDACTED]

DECLASSIFIED

NATIONAL ADVISORY COMMITTEE FOR AERONAUTICS

RESEARCH MEMORANDUM

for the

U. S. Air Force

TRANSONIC AERODYNAMIC CHARACTERISTICS OF A 1/15-SCALE

MODEL OF THE CONVAIR B-58 AIRPLANE

By John M. Swihart

SUMMARY

An investigation of a 1/15-scale model of the Convair B-58 airplane weapons system has been conducted in the Langley 16-foot transonic tunnel. The Convair B-58 airplane has been designed for a long-range subsonic cruise and a supersonic dash. The principles of the area rule were applied in the design.

The Mach number range of the investigation was from 0.80 to 1.12 and the Reynolds number range was from 9.8×10^6 to 10.4×10^6 based on the wing mean aerodynamic chord. The angle-of-attack range was generally from about -5° to 5° and the elevons were not deflected for this investigation.

The results of the investigation indicate that the complete model (airplane plus missile) has a minimum drag coefficient of 0.014 at a Mach number of 0.90 and a transonic rise in drag coefficient of 0.014. The return configuration (airframe only) has a minimum drag coefficient of 0.012 at a Mach number of 0.90 and a transonic rise in drag coefficient of 0.013. It was found that the complete-model drag coefficient was almost exactly the sum of the return configuration and the pod-alone drag coefficients - an outstanding result of the application of the area-rule principles. Comparison of a 1/15-scale free-flight model and the present data indicated excellent agreement. The maximum lift-drag ratio at a Mach number of 0.80 was 11.0 for the return configuration and 10.3 for the complete model. In the low supersonic range, the maximum lift-drag ratio was 7.1 for the return configuration and 6.1 for the complete model.


The aerodynamic-center shift between the subsonic and the low supersonic range was from 32.5 to 44.5 percent of the mean aerodynamic chord for the complete model and from 33.5 to 43.5 percent of the mean aerodynamic chord for the return configuration.

INTRODUCTION

The National Advisory Committee for Aeronautics has carried out extensive research on various models of the Convair B-58 airplane. Reference 1 reported investigations of the original two-engine version and on four models of the advanced four-engine versions. The four-engine versions were designed according to the principles of the transonic area rule (ref. 2). Several models have been tested by the Langley Pilotless Aircraft Research Division. (See refs. 3 to 6.) Pressure distributions on the wing with and without nacelles at supersonic speeds have been obtained at the Ames Laboratory and are reported in reference 7.

The Convair B-58 airplane is a delta-wing bomber-type airplane weapons system designed for a long-range subsonic cruise and a supersonic dash. There are two parts in the airplane weapons system. An airplane with four pylon-mounted single-engine nacelles, a 4-percent-thick delta wing, and a sweptback vertical tail is designated the return configuration. The complete aircraft is the return configuration with an air-to-surface missile mounted on a pylon beneath the fuselage. The Convair B-58 model is very similar to the Convair MX-1964 model with split nacelles (ref. 1) except that both nacelles of the B-58 model were mounted on a pylon on the undersurface of the wing. The four-engine models of reference 1 were designed according to the principles of the transonic area rule, but the return configuration of the B-58 has been designed to an area distribution for a Mach number of 2.0 in a manner similar to that described in reference 8. It should be noted that the Convair B-58 model retains split nacelles, although reference 1 indicated a lower trim drag for two twin-engine nacelles. Unpublished data from Ames Laboratory showed very poor directional stability at supersonic speeds for the twin-engine nacelles and acceptable stability for the split nacelles mounted on the lower surface of the wing. For these reasons particularly, the underslung split nacelles were retained on the Convair B-58 model.

The present investigation at the Langley 16-foot transonic tunnel was made to determine the minimum drag and the drag at cruising lift coefficient of a 1/15-scale model of the Convair B-58 airplane. The investigation was conducted at the request of the United States Air Force. The Mach number range of the investigation was from 0.80 to 1.12 with corresponding Reynolds numbers based on wing mean aerodynamic chord from 9.8×10^6 to 10.4×10^6 . The angle-of-attack range was generally from about -5° to 5° . The elevons were undeflected for this investigation.



SYMBOLS

A	cross-sectional area of nacelle
B	base area of nacelle or fuselage
b	wing span
C_D	external drag coefficient, $\frac{D}{q_o S} = C_{DT} - C_{FB} - C_{FI}$
C_{DT}	balance-measured drag coefficient
C_{FB}	base-force coefficient, $\frac{C_{p_B} B}{S}$
C_{FI}	nacelle internal-force coefficient, $\frac{m(V_o - V_E) - A_E(p_E - p_o)}{q_o S}$
C_L	lift coefficient, $\frac{L}{q_o S}$
C_m	pitching-moment coefficient, $\frac{M_{0.35c'}}{q_o S c'}$
C_p	pressure coefficient, $\frac{p_{local} - p_o}{q_o}$
c'	mean aerodynamic chord
D	external drag
L	lift
l	model length
$M_{0.35c'}$	pitching moment about 0.35c'
M	Mach number
m	mass flow

m'	point mass-flow ratio, $\frac{\rho_E V_E}{\rho_O V_O}$
p	static pressure
q	dynamic pressure
R	Reynolds number
S	wing area
V	velocity
x	distance to rear of nose of fuselage
α	model angle of attack measured from fuselage reference line (fuselage reference line is in parting plane between return configuration and pod pylon)
ρ	mass density

Slope parameters:

$C_{L\alpha}$ lift-curve slope, $\left(\frac{\partial C_L}{\partial \alpha}\right)_{\alpha=0^\circ}$

$\left(\frac{dC_m}{dC_L}\right)_{C_L=0^\circ}$ pitching-moment-curve slope

Subscripts:

B	base
E	nacelle exit station
I	internal
max	maximum
o	free stream

MODEL DESCRIPTION

The model consisted of a fuselage, wing, nacelles, vertical tail, and a removable store or missile called the pod. A sketch of the model with the pod attached is shown in figure 1 and table I gives the model physical characteristics and dimensions. The model was constructed of magnesium castings and polished to a high aerodynamic cleanness. The delta wing had a leading-edge sweep of 60° , a trailing-edge sweep of -10° , an angle of incidence to the fuselage reference line of 3° , and NACA 0004.08-63 airfoil sections parallel to the plane of symmetry. The wing was conically cambered according to a method outlined in references 9 and 10, and the exact details of the conical camber for the wing were given in reference 1.

Movable elevons were built into the wing trailing edge but were positioned at 0° deflection for this investigation. The elevon area for the Convair B-58 model has been decreased from that of the Convair MX-1964 model of reference 1. (See fig. 1.) Landing-gear fairings were cast on the wing upper and lower surfaces as shown on figure 1.


Two pylon-mounted nacelles were attached to the undersurface of each wing at the 0.43b/2 and 0.76b/2 stations. (See figs. 2 and 3.) The inboard nacelle thrust center line was inclined -2° to the wing chord plane (fig. 2) and the outboard nacelle was inclined -4° to the wing chord plane (fig. 3). The nacelle external and internal geometry is shown in figure 4. The nacelle spikes were positioned to duplicate the inlet conditions for cruise at a Mach number of 0.90 and the nacelle spike geometry is shown in figure 5.

The vertical tail had a leading-edge sweepback of 52° , an aspect ratio of 1.32, and a taper ratio of 0.32. It had considerably more area than the Convair MX-1964 tail of reference 1.

The pod was attached to the undersurface of the fuselage with a short pylon. Pod aerodynamic surfaces were a wing, canard, and ventral fin; the wing and canard had the same aspect ratio, taper ratio, and plan form as the main wing. The full-scale air-to-surface missile has a vertical fin which is folded into the pod-support pylon until after pod separation.

TESTS

The operational and flow characteristics of the Langley 16-foot transonic tunnel are reported in reference 11.



DECLASSIFIED

Force data were obtained on the complete model and the return configuration over a Mach number range from 0.80 to 1.12. The angle-of-attack range was from about -5° to 5° and the average Reynolds number based on the wing mean aerodynamic chord was 10.1×10^6 . All force data were obtained with free transition on the model and both the complete model and the return configuration were tested only at an elevon deflection of 0° . Separate runs where no force data were taken were made with the complete model and the return configuration to obtain pressure data in the nacelles since the pressure tubing was carried externally from the nacelles to the fuselage along the upper surface of the wing near the trailing edge.

METHODS

Instrumentation

Forces and moments were measured on an internal six-component balance supported by the tunnel-sting-support system. Fuselage base-pressure forces, nacelle base-pressure forces, and nacelle internal forces were determined from the pressure measurements. Internal pressures were measured near the exits of the inboard and outboard nacelles. Choked flow was obtained in the nacelles at Mach numbers above 0.96.

Data Reduction

All force data were obtained on continuous-operation strip charts and the pressure measurements were recorded photographically. Automatic computing machines were used to reduce the forces and moments to coefficient form after the readings were obtained from the strip charts. Automatic film readers and computers were used to reduce the pressure data to fuselage and nacelle base-pressure forces and nacelle internal forces. All force data presented in this report have been adjusted for base-pressure forces and nacelle internal forces.

Fuselage and nacelle base-force coefficients for the complete model and the return configuration are shown in figure 6. There was only a very small variation of the fuselage base-force coefficient with angle of attack or Mach number for either the complete model or the return configuration. There was considerable variation for the nacelle base-force coefficients with angle of attack and Mach number and the inboard and outboard nacelle variations generally had opposite trends. Nacelle internal-force coefficients are shown in figure 7 for the complete model and the return configuration. The nacelle internal-force coefficients for the inboard and outboard nacelles are practically identical and of small magnitude. The values are lower than those of reference 1 for the

DECLASSIFIED

Convair MX-1964 model, probably a result of shifting the spike position and of slight changes to the internal contour. The point mass-flow ratio m' has not been presented but it remained close to 90 percent for all Mach numbers and angles of attack.

No correction has been made for sting tares. The sting was cylindrical for more than two diameters to the rear of the fuselage base and it is known that sting effects are minimized with this arrangement. The angle of attack has been corrected for sting and balance deflection and for a tunnel upflow angularity of 0.4° that did not vary with Mach number.

In reference 1 the cross plots of drag coefficient against Mach number were faired low in the Mach number range from 1.00 to 1.06 because of tunnel-wall reflected disturbances. No adjustments have been made to the present data because points were obtained at a Mach number of 1.12 and it is estimated that the model was free from tunnel boundary-reflected disturbances at this Mach number.

Accuracy

The values presented in the following table indicate the estimated errors of the data in this paper.

C_L	± 0.01
C_D	± 0.001
C_m	± 0.004
M	± 0.005
α , deg	± 0.1
C_p	± 0.005

A very few errors larger than this estimated accuracy are shown in the basic data and no explanation of why these errors appeared can be given; they were ignored in the fairing of the data.

The complete model was tested; the return configuration was tested; and then the complete model was retested. During these last tests the chord-force strain gage failed; the repeated test data are shown up to the point of failure.

RESULTS AND DISCUSSION

The basic aerodynamic characteristics (α , C_D , and C_m against C_L) are presented in figures 8 and 9 for the complete model and the return

DECLASSIFIED

configuration. The nondimensional cross-sectional area diagrams for the complete model of the B-58 and the MX-1964 split-nacelle model of reference 1 are compared in figure 10. The drag characteristics of the complete model and the return configuration of the B-58 are compared with the MX-1964 split-nacelle model of reference 1 in figure 11.

Drag characteristics.- The purpose of the present investigation was to determine the minimum drag coefficient and the drag at cruising lift coefficient of a 1/15-scale model of the B-58. Figure 11 shows the variation with Mach number of minimum drag coefficient, maximum lift-drag ratio, and lift coefficient for $(L/D)_{\max}$. The data for the complete model are compared with the data for the Convair MX-1964 cambered-wing split-nacelle model of reference 1 and with the return configuration.

The variation of the minimum drag coefficient with Mach number shows that the complete model of the B-58 and the MX-1964 have almost exactly the same minimum-drag-coefficient level (0.014) and transonic drag rise (0.015) up to a Mach number of 1.05 (test limit of ref. 1). The transonic drag rise for the complete model of the B-58 is 0.014 from a Mach number of 0.90 to 1.12. The complete model has a slightly higher drag-coefficient level than the MX-1964 model at a Mach number of 0.90 but had the same level at a Mach number of 1.05. Inspection of the area diagrams shown in figure 10 might indicate a slightly lower level for the B-58 model, since it has a lower total nondimensional area; however, the B-58 model was slightly longer than the MX-1964 model so that the maximum value of A/l^2 was reduced, and the MX-1964 model actually had the lower total cross-sectional area in square feet. The area diagrams indicate very similar forebodies for the two models and only slightly different afterbody slopes; except for other small differences, it might be expected that they would have about the same transonic drag rise.

The minimum drag coefficient for the return configuration is compared with the complete model in figure 11. The return configuration has a minimum drag coefficient of 0.012 at a Mach number of 0.90 and about 0.025 at a Mach number of 1.12. Pod-alone data from reference 12 converted to 1/15-scale model drag coefficients are also shown in figure 11. The difference in model drag coefficient due to the Reynolds number differences between the pod model of reference 12 and the present model would be about 0.0002 based on wing area. With such a small difference in pod drag coefficient due to Reynolds number, it is interesting to compare the complete model, the return configuration, and the return plus the pod minimum drag coefficients. The return configuration was designed for a Mach number of 2.0 and it would not be expected to be optimum at a Mach number of 1.0. Adding the pod to the return configuration gives a Mach number of 1.0 area distribution with the remarkable result that the pod-alone drag coefficient plus the return configuration drag coefficient very nearly equals the complete model drag coefficient at each Mach number. This is certainly an outstanding application of the area-rule principle.

Reference 6 presents drag-coefficient data at model trim lift for a 1/15-scale free-flight model of the B-58 and a comparison of that data with the data of this paper. Figure 12 shows this comparison and is presented to show the excellent agreement that can be obtained between transonic wind-tunnel test data and free-flight data when practically identical models are operated at similar Reynolds numbers.

The variation of lift coefficient for $(L/D)_{\max}$ (fig. 11) indicates that the complete model and the return configuration both attain $(L/D)_{\max}$ at $C_L = 0.25$ at a Mach number of 0.90, which is the design lift coefficient for the subsonic cruise. The variation over the Mach number range is similar to that for the MX-1964 model. It should be noted that the conically cambered wing used on the B-58 model and the MX-1964 model has been designed for an elliptical spanwise loading at a lift coefficient of 0.22 at a Mach number of 1.414.

The value of $(L/D)_{\max}$ is about 11 for the return configuration and about 10.3 for both the complete model of the B-58 and the MX-1964 model at a Mach number of 0.80. The B-58 complete model has a slightly lower $(L/D)_{\max}$ than the MX-1964 at a Mach number of 0.90, probably the result of a slightly higher minimum C_D , but the variation over the Mach number range is very similar. In the low supersonic range, the maximum lift-drag ratio is 6.1 for the complete-model configuration and 7.1 for the return configuration.

When the data of this report are used for performance calculations, the effects of increased Reynolds number and operation of the turbojet engines on the nacelle afterbody and base pressures should be considered. Reference 1 showed that the drag due to lift for this wing was about the theoretical value at a Mach number of 0.90; thus, the drag due to lift could hardly be reduced by increasing the Reynolds number. Therefore, any increase in $(L/D)_{\max}$ at full-scale Reynolds number would be almost entirely the result of lower values of skin-friction drag.

The results of reference 13 indicate that the afterbody and base pressures for a highly boattailed nacelle will be lower than free-stream static pressure when the turbojet engine is operating. It should be expected that the B-58 airplane drag coefficients will be higher and the lift-drag ratios smaller than these model test results where the nacelle base pressures have been adjusted to the condition of free-stream static pressure.

Lift-curve slope.— Figure 13 shows the effect of Mach number on the lift-curve slope for the complete model and the return configuration. The lift-curve slope for the complete model varies from 0.060 to about

DECLASSIFIED

0.074 from a Mach number of 0.80 to a Mach number of 1.00 and then decreases to about 0.063 at a Mach number of 1.12. The lift-curve slope of the return configuration varies in a similar manner over the Mach number range but has a higher slope at a Mach number of 1.12. This result would probably be expected because of a reduction in wave interference when the pod is removed.

Longitudinal stability parameter.- For tailless configurations where flap deflection causes an equal displacement of the pitching-moment curve at each lift coefficient, the aerodynamic center and the neutral point are synonymous. Figure 13 shows the variation of the longitudinal stability parameter dC_m/dC_L or aerodynamic center with Mach number for the complete model and the return configuration. The data indicate that the aerodynamic center or neutral point varies from about 32.5 to 44.5 percent of c' for the complete model and from 33.5 to 43.5 percent of c' for the return configuration over the Mach number range of the investigation. The reason for the larger travel on the complete model is probably the result of the center-of-pressure movement on the pod.

SUMMARY OF RESULTS

An investigation of a 1/15-scale model of the Convair B-58 airplane has been made in the Langley 16-foot transonic tunnel over a Mach number range from 0.80 to 1.12.

The complete model had a subsonic minimum drag coefficient of 0.014 and a transonic rise in minimum drag coefficient of 0.014. The return configuration had a subsonic minimum drag coefficient of 0.012 and a transonic rise in minimum drag coefficient of 0.013. It was found that the complete-model drag coefficient was almost exactly the sum of the return configuration and the pod-alone drag coefficients - an outstanding result of the application of the area-rule principles. Comparison of the drag coefficients at model trim lift from a 1/15-scale free-flight model and the present data indicated excellent agreement. The maximum lift-drag ratio at a Mach number of 0.80 was 11 for the return configuration and 10.3 for the complete model. In the low supersonic range, the maximum lift-drag ratio was 7.1 for the return configuration and 6.1 for the complete model.

The aerodynamic-center shift between the subsonic and the low supersonic range was from 32.5 to 44.5 percent of the mean aerodynamic chord

DECLASSIFIED

for the complete model and from 33.5 to 43.5 percent of the mean aerodynamic chord for the return configuration.

Langley Aeronautical Laboratory,
National Advisory Committee for Aeronautics,
Langley Field, Va., October 9, 1956.

John M. Swihart
John M. Swihart
Aeronautical Research Engineer

Approved:

Eugene C. Draley
Eugene C. Draley
Chief of Full-Scale Research Division

DY

REFERENCES

1. Swihart, John M., and Foss, Willard E., Jr.: Transonic Aerodynamic and Trim Characteristics of a Multi-Engine Delta-Wing Airplane Model. NACA RM L55I27b, 1955.
2. Whitcomb, Richard T.: A Study of the Zero-Lift Drag-Rise Characteristics of Wing-Body Combinations Near the Speed of Sound. NACA Rep. 1273, 1956. (Supersedes NACA RM L52H08.)
3. Hall, James Rudyard: Drag Measurements on Equivalent Bodies of Revolution of Six Configurations of the Convair MX-1964 (Originally MX-1626) Proposed Supersonic Bomber. NACA RM SL53K04, U. S. Air Force, 1953.
4. Hall, James R., and Hopko, Russell N.: Drag and Static Stability at Low Lift of Rocket-Powered Models of the Convair MX-1626 Airplane at Mach Numbers From 0.7 to 1.5. NACA RM SL53F09a, U. S. Air Force, 1953.
5. Hopko, Russell N., Piland, Robert O., and Hall, James R.: Drag Measurements at Low Lift of a Four-Nacelle Airplane Configuration Having a Longitudinal Distribution of Cross-Sectional Area Conducive to Low Transonic Drag Rise. NACA RM L53E29, 1953.
6. Hopko, Russell N., and Kinard, William H.: Drag at Model Trim Lift of a 1/15-Scale Convair B-58 Supersonic Bomber. NACA RM SL56G23, U. S. Air Force, 1956.
7. Phelps, E. Ray: Pressure Distributions at Mach Numbers of 1.6 and 1.9 of a Conically Cambered Wing of Triangular Plan Form With and Without Pylon-Mounted Engine Nacelles. NACA RM A56B03, 1956.
8. Whitcomb, Richard T., and Fischetti, Thomas L.: Development of a Supersonic Area Rule and an Application to the Design of a Wing-Body Combination Having High Lift-to-Drag Ratios. NACA RM L53H31a, 1953.
9. Hall, Charles F.: Lift, Drag, and Pitching Moment of Low-Aspect-Ratio Wings at Subsonic and Supersonic Speeds. NACA RM A53A30, 1953.
10. Boyd, John W., Migotsky, Eugene, and Wetzell, Benton E.: A Study of Conical Camber for Triangular and Sweptback Wings. NACA RM A55G19, 1955.
11. Ward, Vernon G., Whitcomb, Charles F., and Pearson, Merwin D.: Air-Flow and Power Characteristics of the Langley 16-Foot Transonic Tunnel With Slotted Test Section. NACA RM L52E01, 1952.

DECLASSIFIED

12. Hopko, Russell N.: Drag Near Zero Lift of a 1/7-Scale Model of the Convair B-58 External Store as Measured in Free Flight Between Mach Numbers of 0.8 and 2.45. NACA RM SL55G22a, U. S. Air Force, 1955.
13. Henry, Beverly Z., Jr., and Cahn, Maurice S.: Preliminary Results of an Investigation at Transonic Speeds To Determine the Effects of a Heated Propulsive Jet on the Drag Characteristics of a Related Series of Afterbodies. NACA RM L55A24a, 1955.

TABLE I.- PHYSICAL CHARACTERISTICS OF 1/15-SCALE CONVAIR B-58 MODEL

Fuselage:	
Length, in.	69.93
Overall length from nose to tip of vertical tail, in.	75.93
Nacelles:	
Length, in.	19.33
Inlet diameter, in.	1.80
Total inlet area, sq in.	2.54
Net inlet area, sq in.	1.92
Exit diameter, in.	1.69
Exit area, sq in.	2.24
Location of inboard nacelle inclined -2° to wing-chord plane	0.43b/2
Location of outboard nacelle inclined -4° to wing-chord plane	0.76b/2
Spike diameter at inlet, in.	0.34
Wing:	
Span, in.	45.49
Root chord, in.	43.41
Mean aerodynamic chord, in.	28.94
Area, sq ft	6.86
Airfoil section	NACA 0004.08-63
Leading-edge sweep, deg	60
Trailing-edge sweep, deg	-10
Dihedral, deg	0
Incidence, deg	3
Aspect ratio	2.10
Taper ratio	0
Pod:	
Length, in.	44.60
Maximum diameter of body of revolution, in.	4.00
Pod wing:	
Span, in.	13.70
Area, sq ft	0.62
Airfoil section	NACA 0004.5-64
Pod canard:	
Span, in.	7.86
Area, sq ft	0.20
Airfoil section	NACA 0004.5-64
Pod ventral fin:	
Span, in.	4.1
Area, sq ft	0.13
Aspect ratio	1.75
Taper ratio	0.35
Leading-edge sweep, deg	60
Airfoil section	NACA 0005-64
Vertical tail:	
Area, sq ft	0.71
Span, in.	11.60
Aspect ratio	1.32
Taper ratio	0.32
Leading-edge sweep, deg	52
Airfoil section	NACA 0005-64

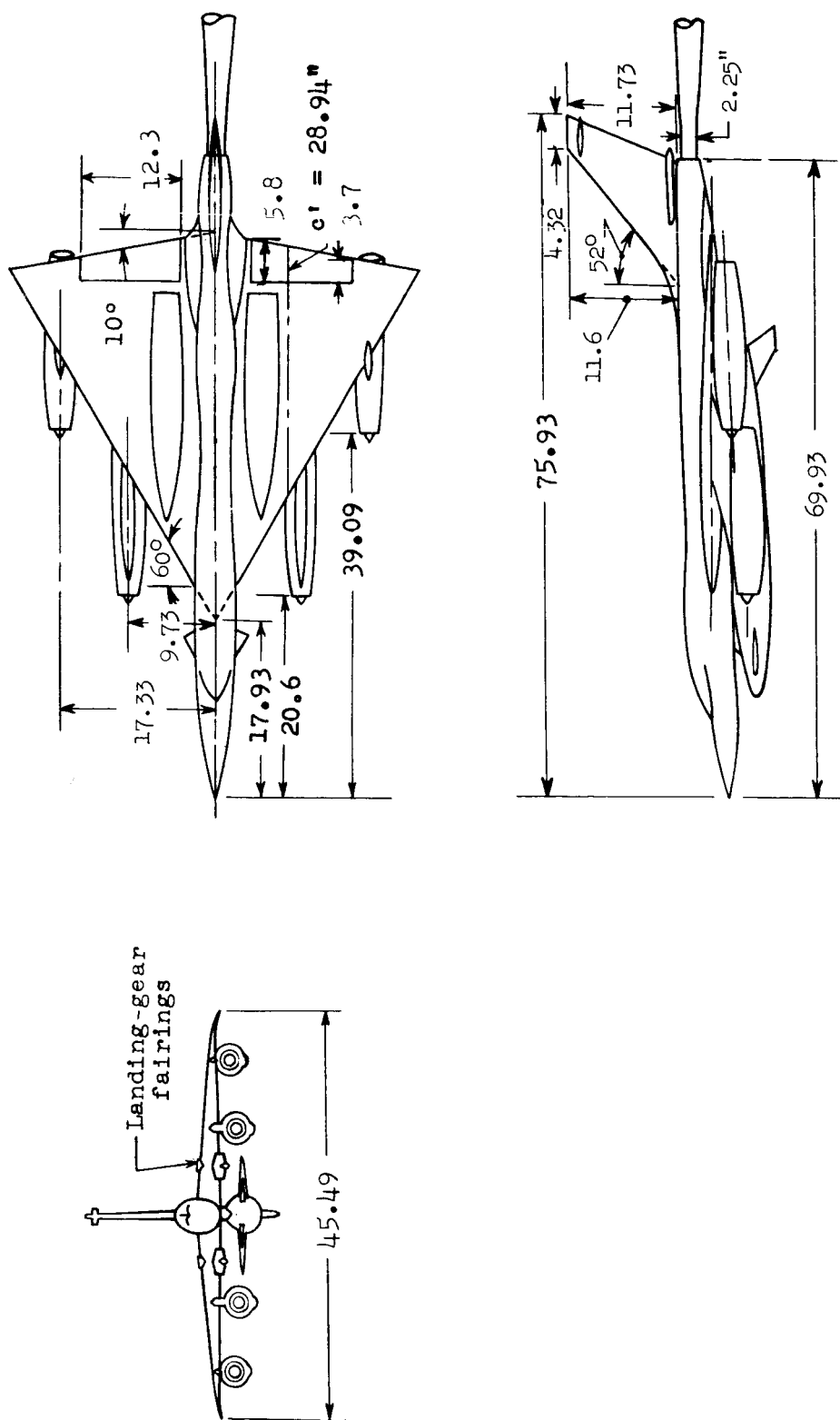


Figure 1.- General arrangement of model. All dimensions are in inches.

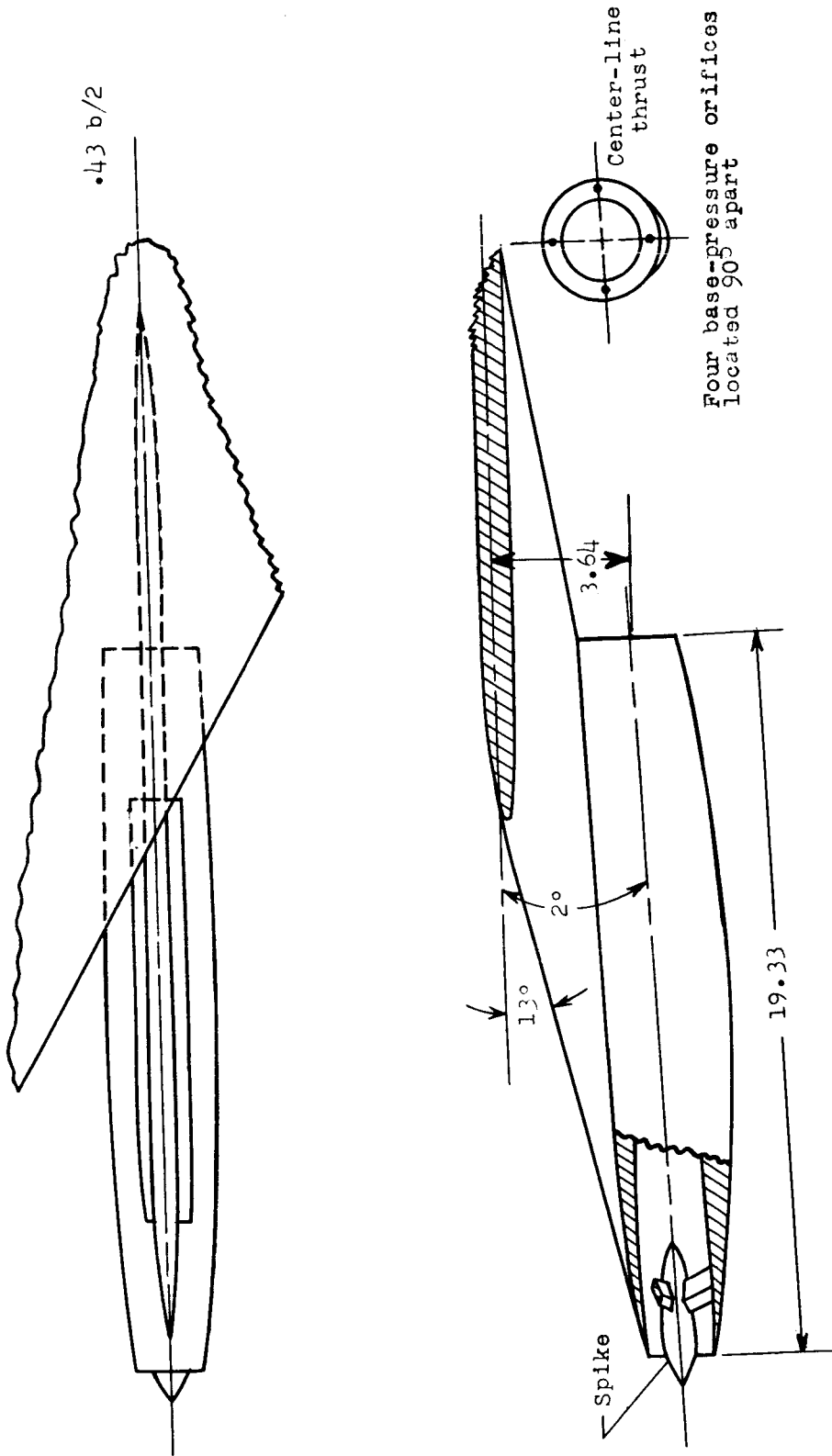


Figure 2.- Inboard nacelle and strut.

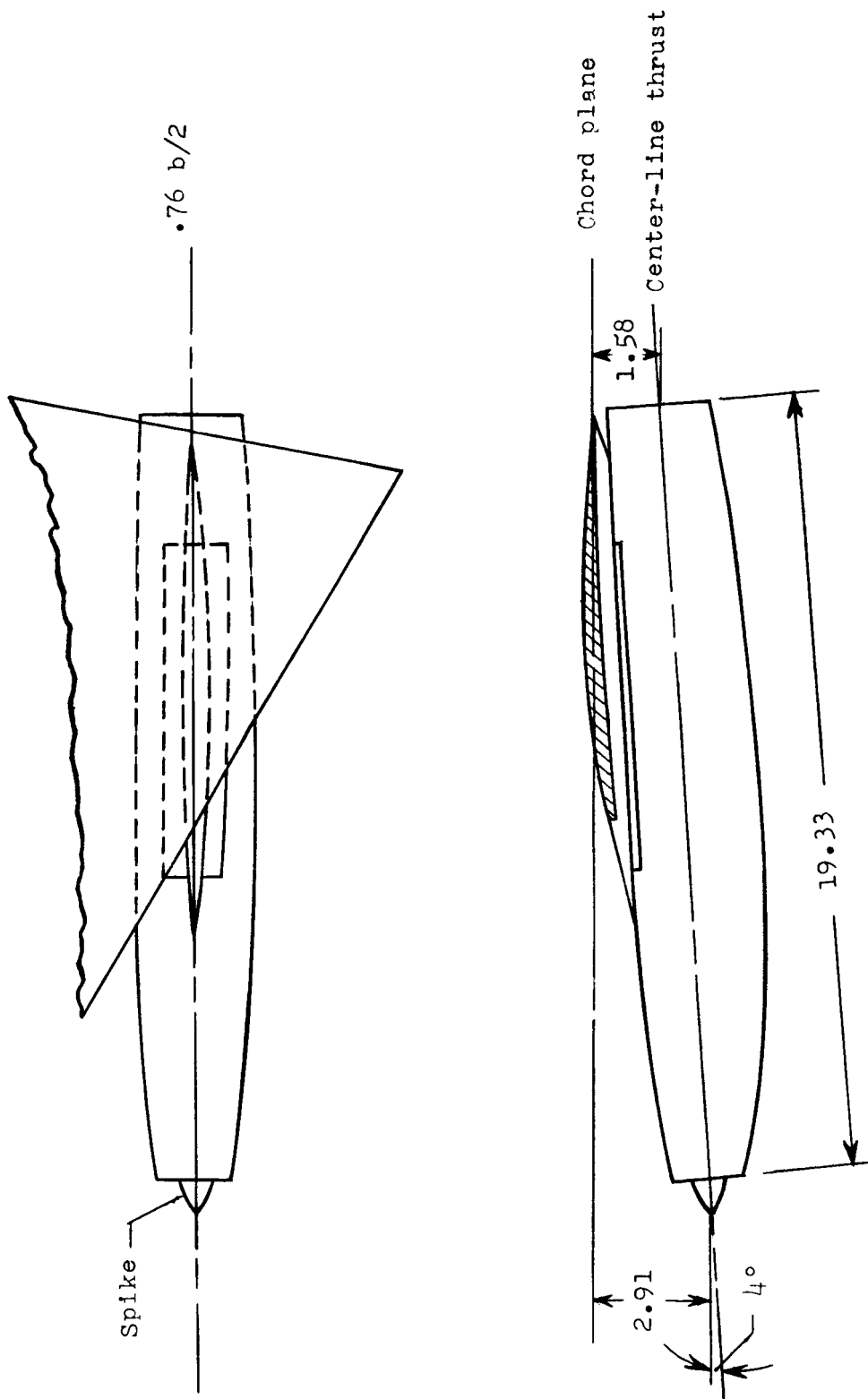
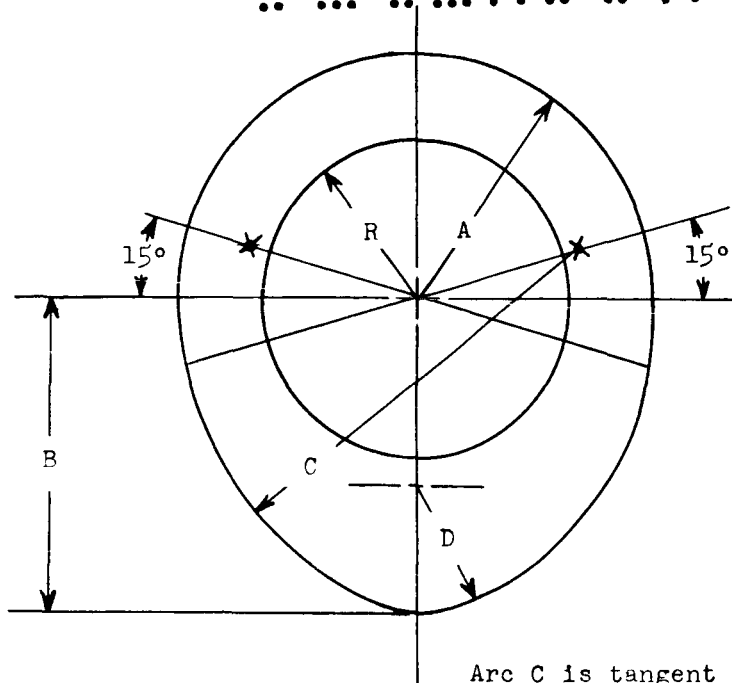


Figure 3.- Outboard nacelle and strut.

[REDACTED]

DECLASSIFIED

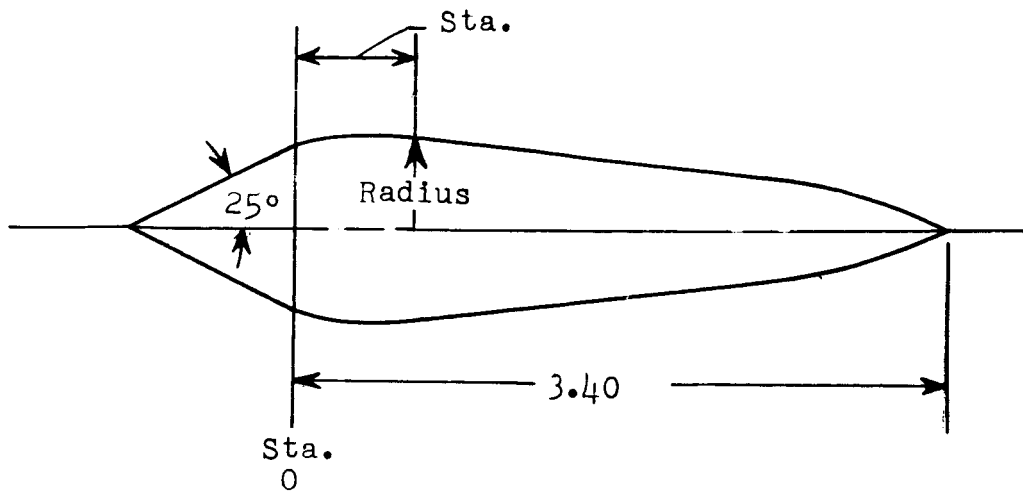


Arc C is tangent to radius A at the 15° line below the thrust line and is tangent to radius D.

Nacelle geometry				Nacelle internal geometry	
Station, in.	Radius A, in.	B, in.	Radius D, in.	Station, in.	Radius R, in.
0.124	0.997	0.997		0.124	0.997
.134	1.007	1.007	0.800	.134	.987
.149	1.015	1.015	.800	.149	.982
.170	1.019	1.019	.800	.170	.980
.333	1.049	1.052	.800	.184	.979
.666	1.100	1.115	.800	.197	.979
1.333	1.172	1.242	.800	.453	.985
2.000	1.219	1.360	.800	15.866	.985
2.667	1.254	1.475	.800	18.667	.878
4.000	1.307	1.669	.800	19.333	.845
6.000	1.381	1.869	.800		
8.000	1.447	1.966	.800		
10.000	1.487	1.971	.800		
10.666	1.491	1.961	.800		
12.000	1.486	1.919	.800		
14.000	1.449	1.802	.800		
16.000	1.399	1.621	.800		
18.000	1.369	1.455	.800		
18.667	1.367	1.409	.800		
19.333	1.367	1.367			

Figure 4.- Nacelle external and internal geometry.

[REDACTED]

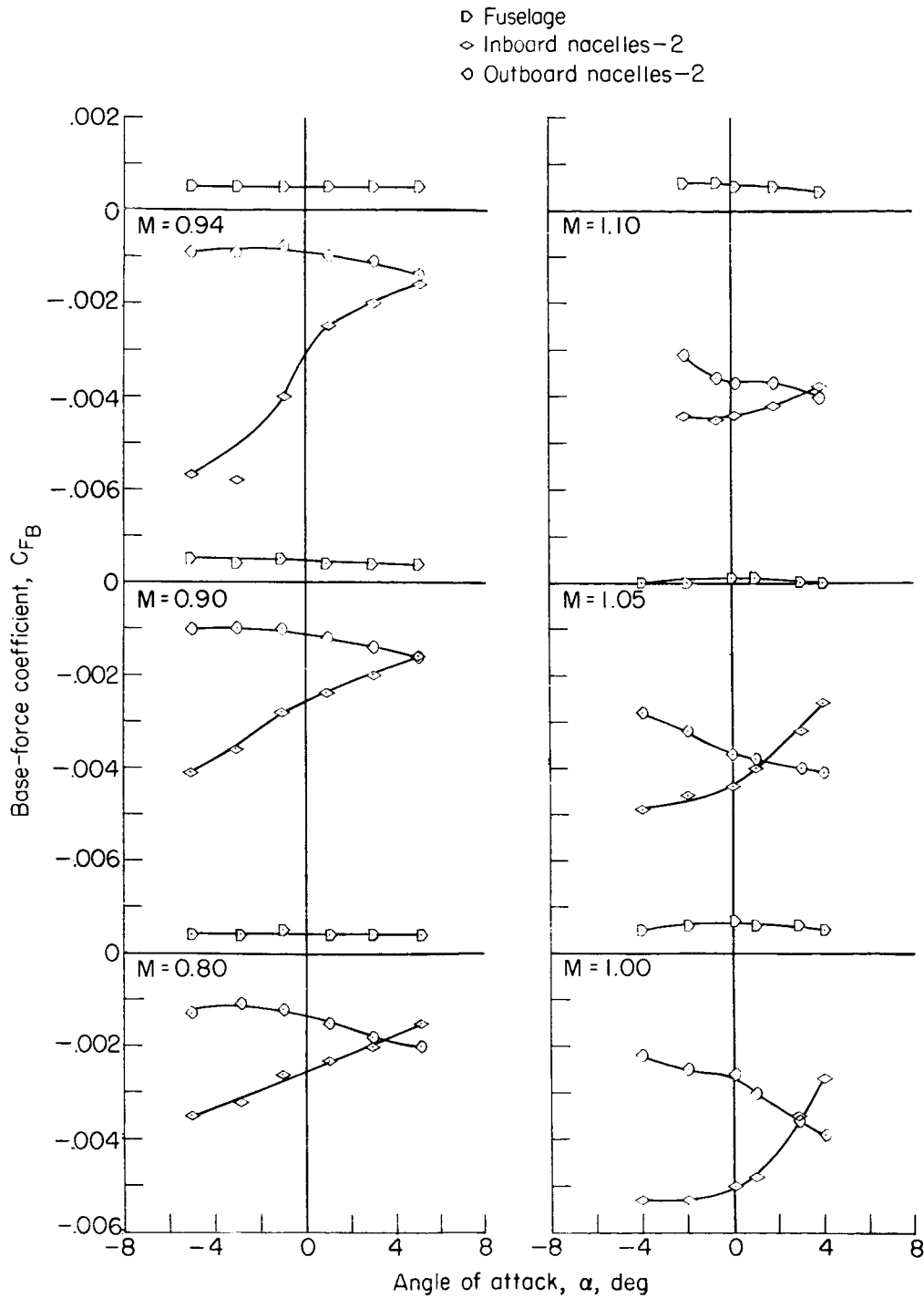


Spike Geometry

Sta.	Radius
- 0.955	0.000
0.000	.445
.113	.474
.227	.486
.340	.478
.453	.469
.567	.458
1.133	.399
1.700	.342
2.267	.283
2.833	.214
2.947	.181
3.060	.136
3.173	.091
3.287	.045
3.400	.000

Figure 5.- Nacelle spike geometry.

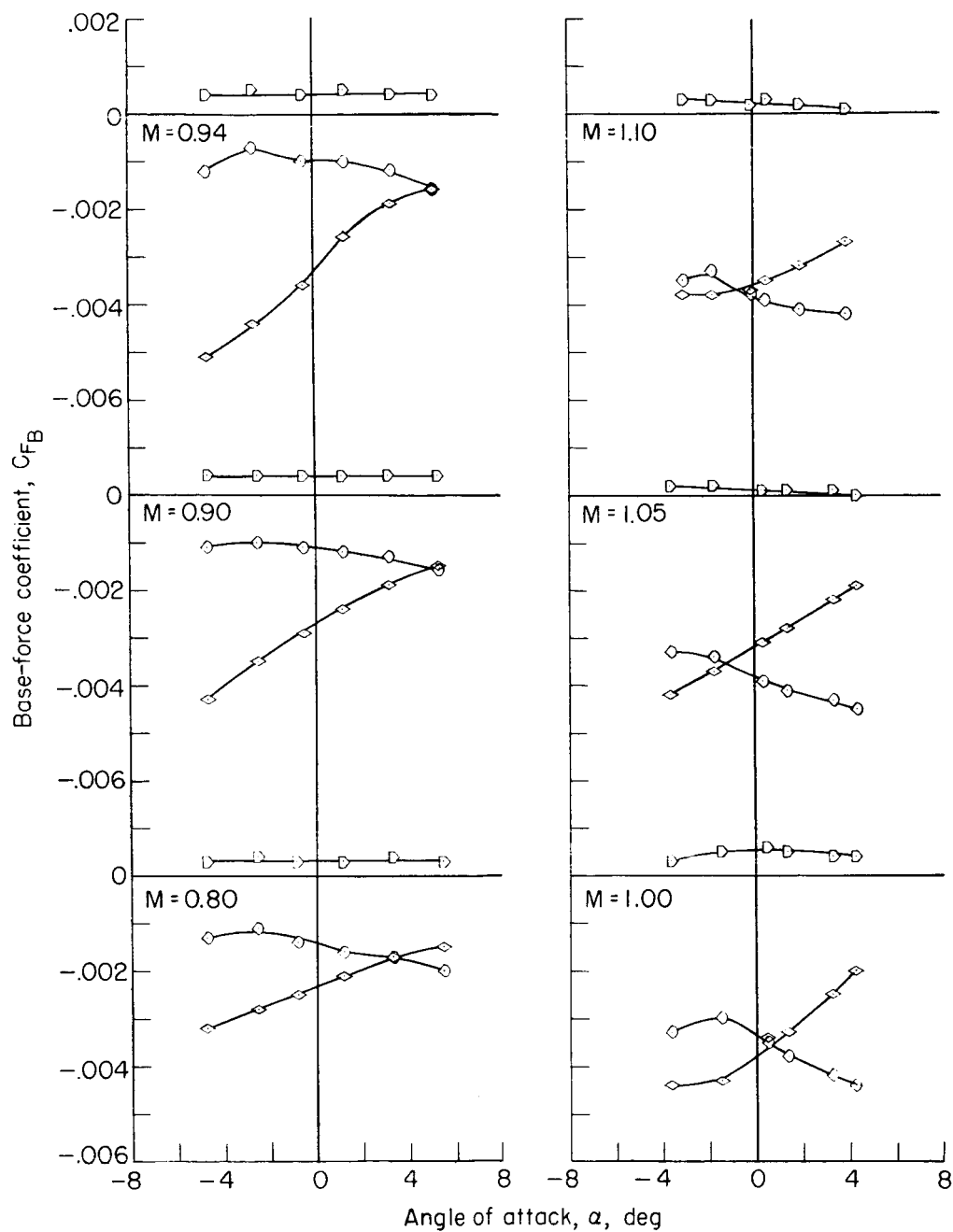
DECLASSIFIED



(a) Complete model.

Figure 6.- Variation of base-force coefficient with angle of attack for 1/15-scale model of the Convair B-58 airplane.

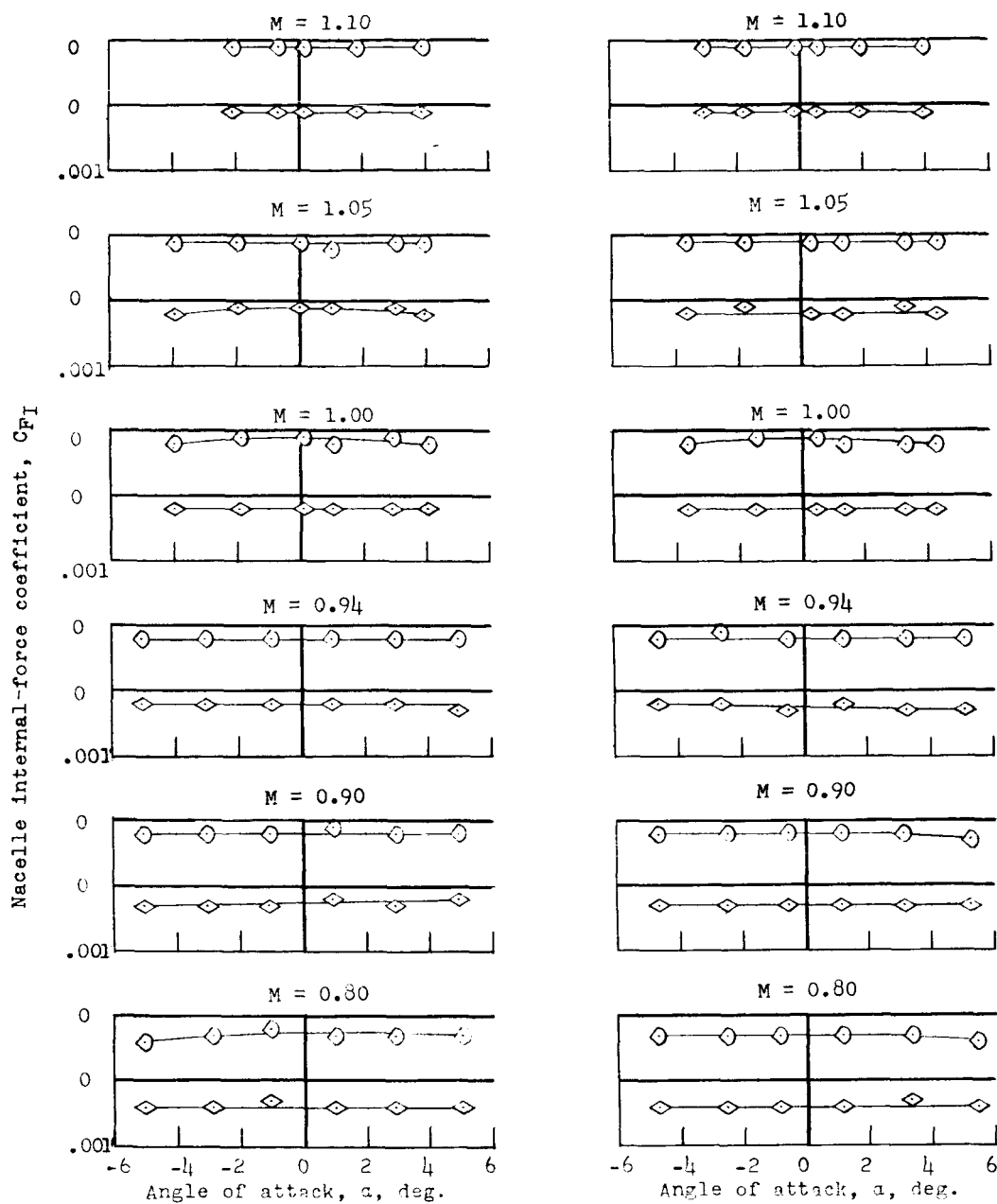
- ◇ Fuselage
- ◇ Inboard nacelles-2
- ◇ Outboard nacelles-2



(b) Return configuration.

Figure 6.- Concluded.

◇ Outboard nacelles
 ◇ Inboard nacelles



(a) Complete model.

(b) Return configuration.

Figure 7.- Variation of nacelle internal-force coefficient with angle of attack for 1/15-scale model of the Convair B-58 airplane.

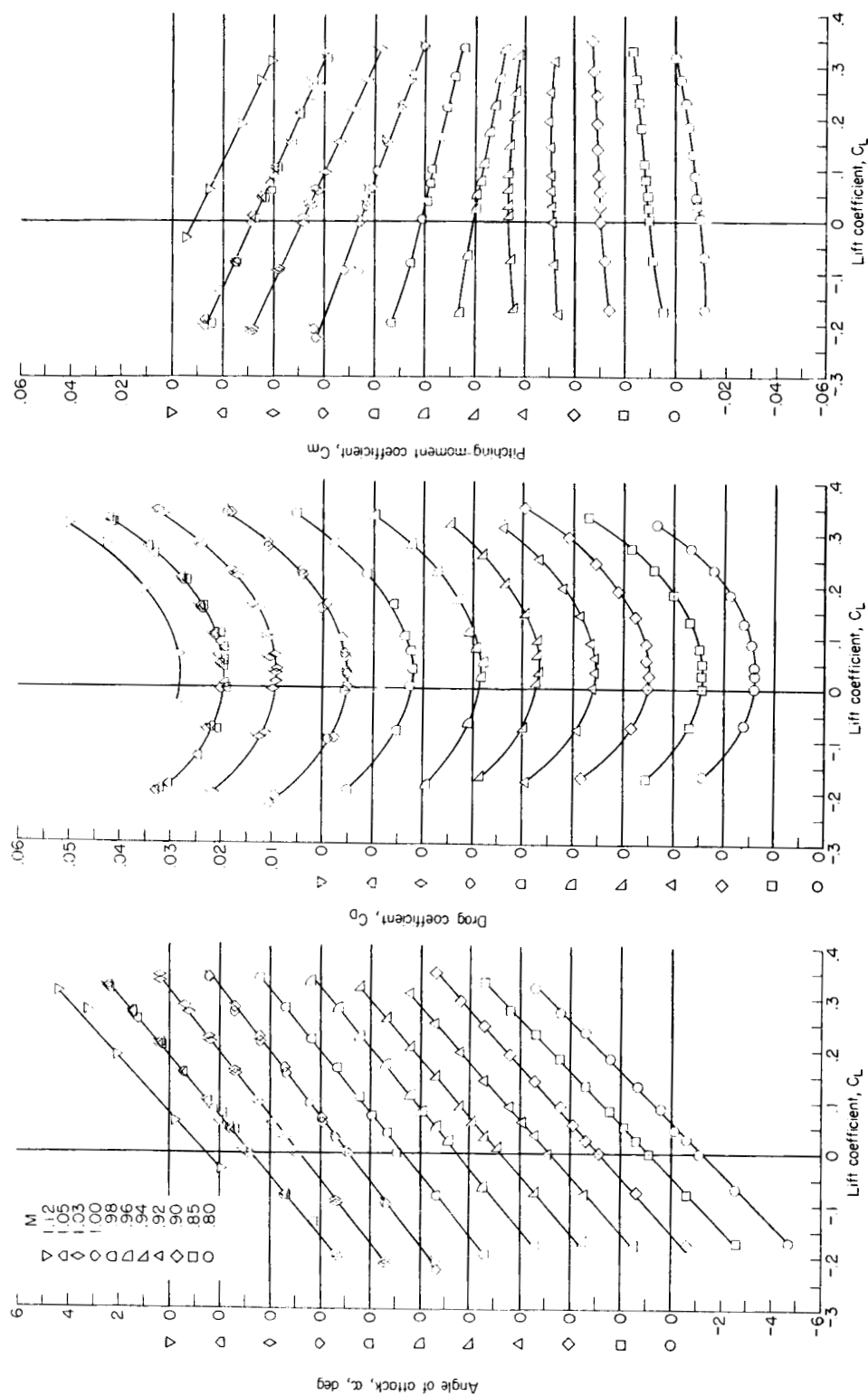


Figure 8.- Aerodynamic characteristics of the complete model of the Convair E-58 airplane.
Flagged symbols are repeat runs.

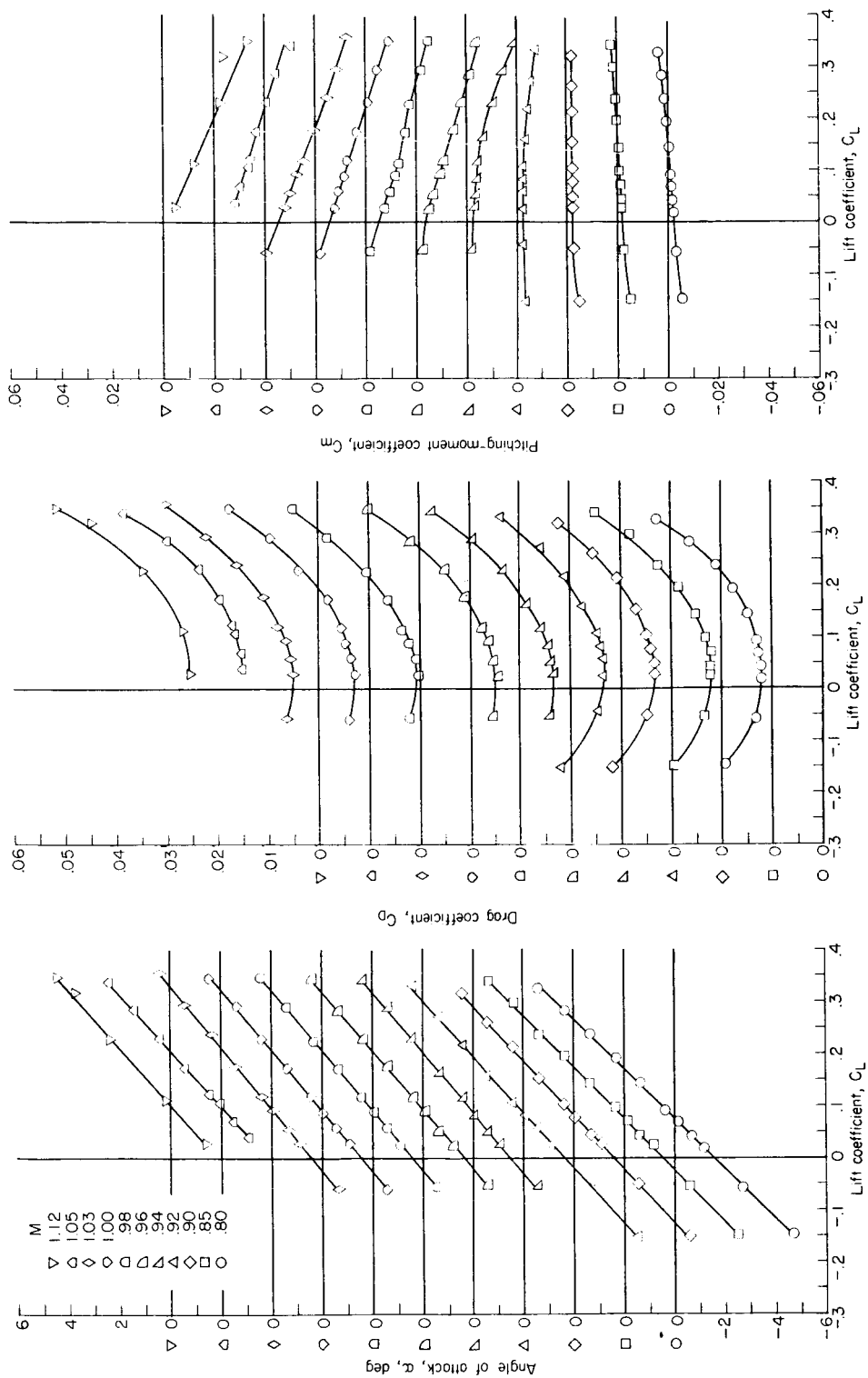
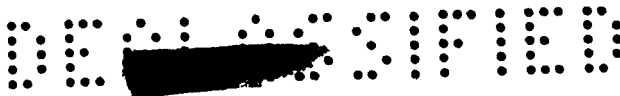


Figure 9.- Aerodynamic characteristics of the return configuration of the Convair B-58 airplane.

REF ID: A56J22

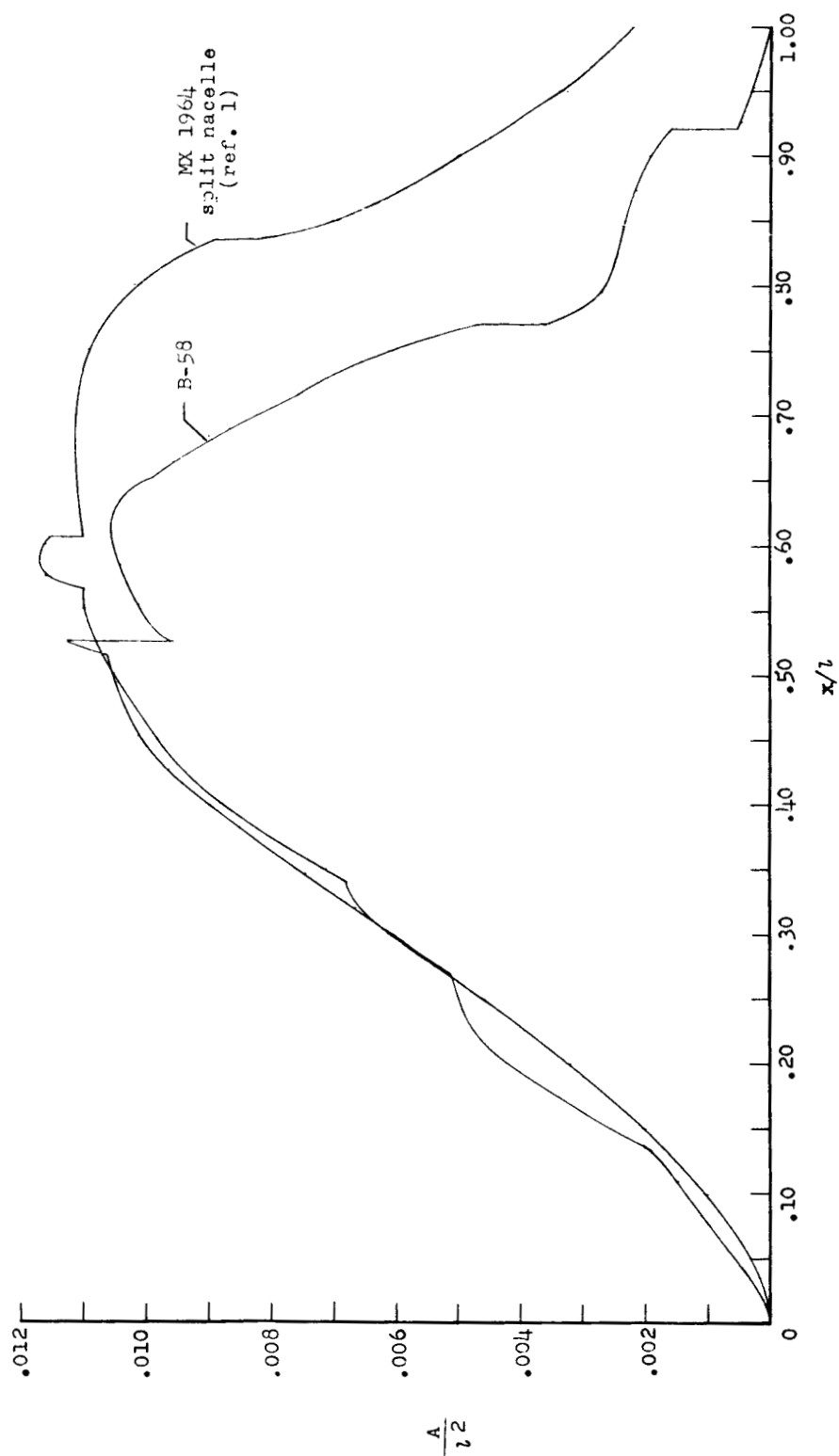


Figure 10.- Nondimensional area distributions for 1/15-scale models of the Convair B-58 and Convair MX-1964 airplanes.

DECLASSIFIED

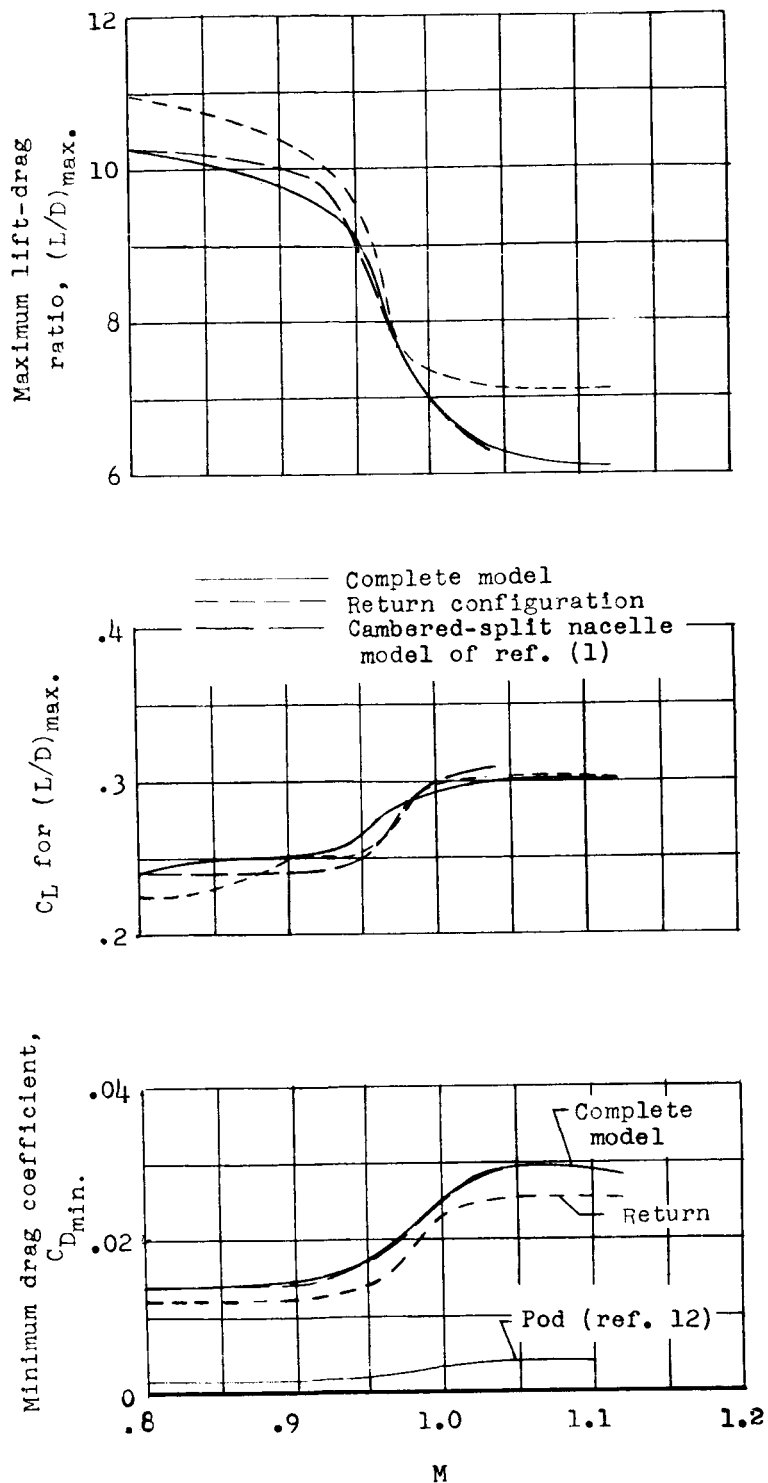


Figure 11.- Drag characteristics of the Convair B-58 model and a comparison with the Convair MX-1964 model of reference 1.

CONFIDENTIAL

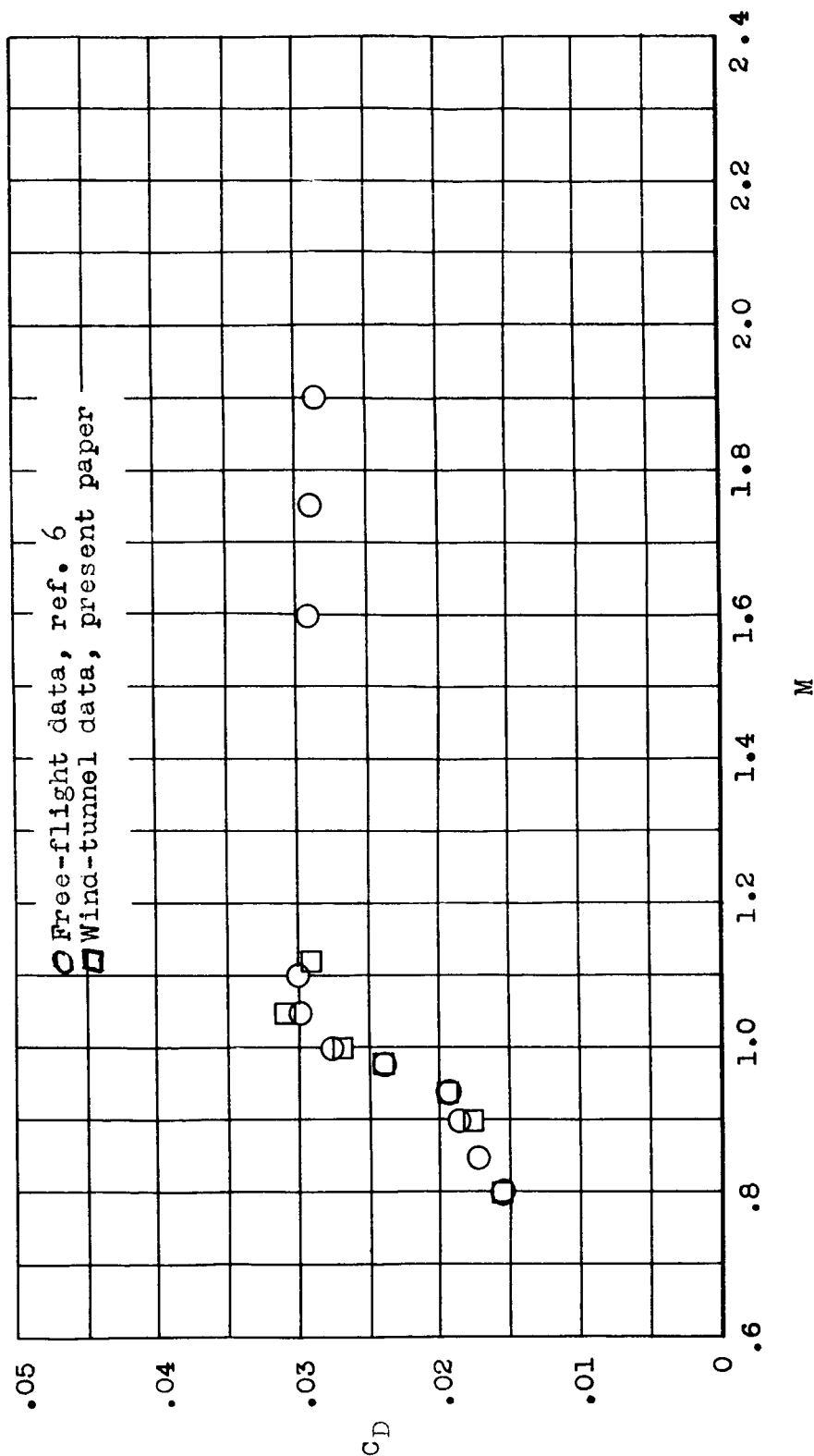


Figure 12.- Comparison of free-flight data of reference 6 and the wind-tunnel data on a 1/15-scale model of the Convair B-58 airplane at model trim lift. Complete model.

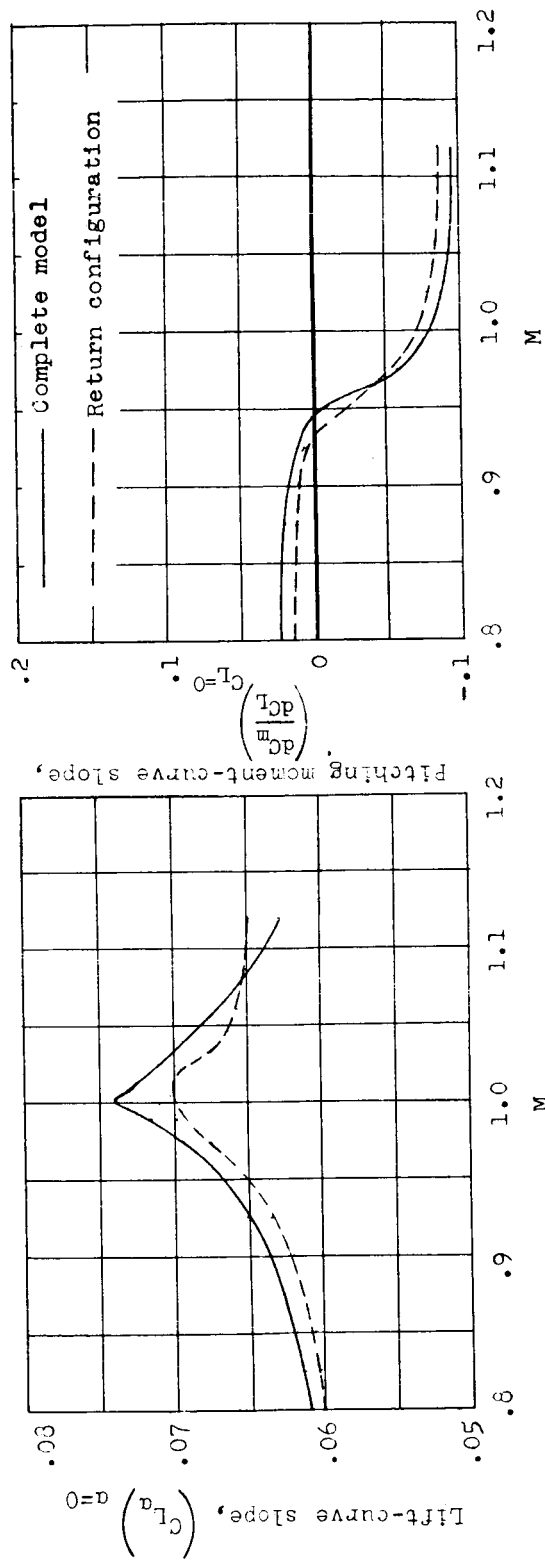


Figure 13.- Effect of Mach number on lift-curve slope and pitching-moment-curve slope.

REF ID: A60000

INDEX

<u>Subject</u>	<u>Number</u>
Airplanes - Components in Combination	1.7.1.1
Wing-Nacelle Combinations - Airplanes	1.7.1.1.2
Airplanes - Specific Types	1.7.1.2
Airplanes - Performance	1.7.1.3
Missiles - Components in Combination	1.7.2.1

ABSTRACT

An investigation of a 1/15-scale model of the Convair B-58 airplane weapons system has been conducted in the Langley 16-foot transonic tunnel.

The results indicate that the complete model (airplane plus missile) drag coefficient was almost exactly the sum of the return configuration (airplane only) drag coefficient and the pod-alone drag coefficient - an outstanding result of the application of the area-rule principles.